

Holographic Intelligence Surface Assisted Integrated Sensing and Communication

Zhuoyang Liu, *Graduated Student Member, IEEE*, Yuchen Zhang, *Graduated Student Member, IEEE*, Haiyang Zhang, *Member, IEEE*, Feng Xu, *Senior Member, IEEE*, and Yonina C. Eldar, *Fellow, IEEE*

Abstract—Traditional discrete-array-based systems fail to exploit interactions between closely spaced antennas, resulting in inadequate utilization of the aperture resource. In this paper, we propose a holographic intelligence surface (HIS) assisted integrated sensing and communication (HISAC) system, wherein both the transmitter and receiver are fabricated using a continuous-aperture array. A continuous-discrete transformation of the HIS pattern based on the Fourier transform is proposed, converting the continuous pattern design into a discrete beamforming design. We formulate a joint transmit-receive beamforming optimization problem for the HISAC system, aiming to balance the performance of multi-target sensing while fulfilling the performance requirement of multi-user communication. To solve the non-convex problem with coupled variables, an alternating optimization-based algorithm is proposed to optimize the HISAC transmit-receive beamforming in an alternate manner. Specifically, the transmit beamforming design is solved by decoupling into a series of feasibility-checking sub-problems while the receive beamforming is determined by the Rayleigh quotient-based method. Simulation results demonstrate the superiority of the proposed HISAC system over traditional discrete-array-based ISAC systems, achieving significantly higher sensing performance while guaranteeing predetermined communication performance.

Index Terms—Holographic intelligence surface, integrated sensing and communication, pattern design strategy, continuous-aperture array

I. INTRODUCTION

Integrated sensing and communication (ISAC) system, which envisions simultaneous sensing and communication on a shared waveform/platform, is considered a vital solution for tackling challenges associated with spectral and/or power efficiency in 6G wireless networks [1], [2]. For the ISAC waveform design, former studies advocate a joint design paradigm [3]–[8]. Instead of allocating orthogonal temporal/spectral/spatial resources to sensing and communication functionalities [9]–[11], joint design achieves ISAC by a single waveform with non-orthogonal resources, which not only enhances spectral efficiency but also yields a flexible performance tradeoff between sensing and communication [3]–[8]. In a multi-antenna setting, joint ISAC waveform design is typically achieved through transmit beamforming/precoding design. This entails designing spatial beamformers/precoders

judiciously to maximize sensing/communication under performance constraints in communication/sensing, thereby striking a balance between the two functionalities [3]–[5]. Furthermore, by leveraging radar receivers, joint transmit-receive beamforming has been proposed in the literature to further enhance ISAC performance [6]–[8].

The aforementioned beamforming designs in ISAC systems typically rely on discrete antenna arrays, where the antenna spacing is constrained to half-wavelength. This limits the number of antennas for a given aperture, thereby resulting in insufficient exploitation of array gain for ISAC performance enhancement [12], [13]. In addition, modeling electromagnetic (EM) propagation for the discrete array usually overlooks the mutual interference between two closely spaced antennas, potentially leading to inadequate information acquisition during signal reception [14], [15]. To overcome these limitations, the concept of holographic intelligence surface (HIS), also known as holographic multiple-input multiple-output (MIMO) [16], [17] and continuous-aperture MIMO [18], [19], has emerged. Unlike the discrete array consisting of multiple patch antennas with half-wavelength spacing, HIS achieves a quasi-continuous-aperture array by deploying massive sub-wavelength tunable elements in a compact space, which yields high array gain with limited size [20]. The advantages of HIS include enhancing signal coverage [21], improving communication rate [22], and boosting localization accuracy [13], [23]. However, due to its continuous nature, HIS incurs significant challenges for array signal processing, making traditional beamforming techniques [3]–[8], which are tailored for discrete arrays, inefficient or even inapplicable [16], [17]. Due to these challenges, integrating HIS into the ISAC system, though promising for achieving a better performance trade-off between sensing and communication, is still in its infancy.

The primary goals of this work are to: 1) design an HIS-assisted ISAC (HISAC) transceiver architecture, 2) develop an HISAC transmit-receive beamforming framework, and 3) demonstrate the performance gain by employing HIS instead of traditional discrete arrays in ISAC systems.

A. Prior work

Many efforts have been dedicated to beamforming design for the ISAC systems [3]–[8], [24]–[29], including transmit beamforming and joint transmit-receive beamforming. Transmit beamforming builds on the spatial degrees of freedom (DoFs) at the transmitter, which is devised to strike performance trade-off between sensing and communication [3]–[5], [24]. A commonly adopted strategy of transmit beamforming is to modify the transmit beam by optimizing the beamformer, aiming to maximize the power sent towards the targets while

Z. Liu and F. Xu are with the Key Lab for Information Science of Electromagnetic Wave (MoE), Fudan University, Shanghai 200433, China (e-mail: {liuzy20; fengxu}@fudan.edu.cn).

Y. Zhang is with the National Key Laboratory of Wireless Communications, University of Electronic Science and Technology of China, Chengdu 611731, China (e-mail: yc_zhang@std.uestc.edu.cn).

H. Zhang is with the School of Communication and Information Engineering, Nanjing University of Posts and Telecommunications, Nanjing 210003, China (e-mail: haiyang.zhang@njupt.edu.cn).

Y. C. Eldar is with the Faculty of Math and CS, Weizmann Institute of Science, Rehovot 7610001, Israel (e-mail: yonina.eldar@weizmann.ac.il).

fulfilling the communication performance requirement at each user [3]–[5], [24], [25].

Transmit beamforming fails to explore the spatial DoFs at the radar receiver, which holds potential to further enhance ISAC performance. Joint transmit-receive beamforming, in which the transmitter-side beamformers and radar receiver-side beamformers/filters are designed simultaneously, has been proposed in [6]–[8], [26]–[30]. The authors of [8] employed the Cramér-Rao bound (CRB) as the radar performance indicator and optimized the CRB while meeting the user signal-to-interference-and-noise ratio (SINR) requirement. However, explicit receive beamforming was not addressed. In [26], the authors considered transmit-receive beamforming in ISAC systems with SINR being the radar performance metric. However, without being optimized adaptively, the receive beamforming conducted at the radar receiver was solely determined by the steering vector. As a step further, [30] proposed a design framework for ISAC transmit-receive beamforming, optimizing transmit and receive beamformers alternately. The aforementioned works regarding ISAC beamforming typically rely on a discrete array, which limits performance due to inefficient utilization of a given aperture [14], [15].

With the development of continuous-aperture array technology, HIS has been devised to alleviate the performance bottleneck caused by traditional discrete arrays, enabling higher array gain for a given aperture size [12]–[17]. The superiority of HIS has been demonstrated in various systems aimed at different tasks [18], [20]–[22], [31], [32]. For instance, the channel model and performance bounds of HIS-based multi-user MIMO systems were analyzed in [21], [33], [34]. To characterize the radiation model of HIS, it is necessary to design the surface pattern, known as the current density distribution, for a continuous-aperture array [16]–[19]. The authors of [16]–[18], [34], [35] modeled the radiation of continuous-aperture arrays and derived a closed-form expression of the capacity between two continuous volumes by utilizing the Fourier basis functions of continuous-space EM channels. To optimize the capacity of HIS-based communications, a Fourier transform-based pattern design approach was proposed by [19]. Specifically, a pattern division multiplexing (PDM) method was developed to model the radiation for HIS, aiming to maximize the sum rate when serving multiple communication users with HIS. Compared to [16]–[18], [34], [35] that employed the standard basis functions and projection coefficient matrices of the Fourier transform, the pattern design in [19] differed in incorporating additional optimizable projection coefficient matrices. This modification enhances the flexibility of HIS radiation modeling and pattern design, effectively addressing the issue of infinite computation resulting from the continuous nature of HIS.

B. Motivation and Contribution

Most existing works employing HIS have focused on communication tasks [19], [21], [22], [31], [32], [36], whereas the incorporation of HIS into ISAC systems has remained in its infancy [20], [37], [38]. Although the advantages of deploying sub-half-wavelength-spacing antennas for ISAC systems have

been initially revealed in [20], [37], the advocated antenna array remained discrete. Therefore, the proposed schemes are not applicable to HISAC systems comprised of continuous-aperture arrays.

To fill the gap, this work focuses on incorporating HIS into ISAC system. Specifically, we propose an ISAC transceiver structure based on HIS, wherein both the transmitter and receiver of the base station (BS) are fabricated using HISs. By generating a specific pattern of the HIS, the radiation of the EM waves can be configured to meet the requirements of both sensing and communication. However, due to its continuity, the pattern of the HIS has infinite dimensions. Inspired by [19], we develop a continuous-discrete transformation based on the Fourier transform, which converts the continuous current from the space domain into the discrete wavenumber domain. Then, the problem of pattern design is transformed into a joint transmit-receive beamforming problem, where projection/beamforming matrices of the pattern in the wavenumber domain are optimizable to configure the beams of HISs. Based on this, we jointly design the transmit-receive beamformers by optimizing their coefficient matrices, maximizing the minimal sensing SINR among multiple targets while guaranteeing multi-user communication SINR requirements.

Due to the non-convex max-min objective function and coupled optimization variables of the joint transmit-receive design, the formulated problem is non-convex and, consequently, challenging to solve. We propose an alternating optimization (AO) algorithm to address it by designing the HIS transmit the receive beamforming iteratively. Specifically, we propose an adaptive bisection searching (ABS) method to accelerate the convergence of the semidefinite relaxation (SDR)-based bisection iteration process in the HIS transmit beamforming. Additionally, we propose a Rayleigh quotient-based algorithm for configuring the HIS receive beamforming. Numerical results demonstrate that our proposed HISAC system enhances the performance of both sensing and communication compared to the discrete array-based counterpart system.

The main contributions of this work are summarized as follows:

- **HISAC Transceiver:** To the best of our knowledge, we are the first to propose the HISAC system, where the transmit HIS supports multi-user communication and illuminates multiple radar targets, and the receive HIS collects the radar echoes. Specifically, we study the joint design of transmit HIS and receive HIS, balancing the performance of sensing and communication in the proposed system.
- **Continuous-Discrete Transformation:** We convert the HIS pattern from the continuous space domain into the discrete wavenumber domain, through which the joint transmit-receive beamforming can be efficiently designed. Based on the continuous-discrete transformation, we formulate an optimization problem concerning the joint transmit-receive beamforming design for HISAC, balancing multi-target sensing performance while fulfilling multi-user communication performance requirements.
- **Joint Transmit-Receive Beamforming in HISAC:** We develop an AO algorithm by recasting the original problem into: transmit HIS design and receive HIS config-

uration. Due to the high complexity of the involved SDR-based bisection search method, we propose an ABS method to obtain the refined potential range of the bisection search and accelerate the convergence in the iteration process. To address the receive HIS configuration, bluea Rayleigh quotient-based method is proposed obtaining a closed-form solution.

- **Performance:** Numerical results reveal the significant performance gain of the proposed HISAC system, over its discrete-array-based counterpart. Specifically, the proposed schemes achieve a remarkable 9.5 dB sensing SINR gain compared to the discrete-based arrays under the same communication SINR requirement.

C. Organization and Notation

The rest of the paper is organized as follows: Section II presents the HISAC system and formulates a pattern design problem. The continuous-discrete transformation is developed to convert the continuous pattern design into a joint transmit-receive beamforming problem in Section III. Section IV presents efficient methods to optimize patterns of both the transmit HIS and the receive HIS. Section V numerically demonstrates the solution and evaluates its performance in different settings. Finally, Section VI concludes the paper.

Throughout the paper, we use boldface lower-case and upper-case letters for vectors and matrices, respectively. The maximal eigenvalue of the matrix \mathbf{A} is denoted by $\lambda_{max}(\mathbf{A})$. The ℓ_2 norm, Frobenius norm, conjugate operation, transpose, Hermitian transpose, and stochastic expectation are written as $\|\cdot\|_2$, $\|\cdot\|_F$, $(\cdot)^*$, $(\cdot)^T$, $(\cdot)^H$, and $\mathbf{E}(\cdot)$, respectively. We use \mathbf{I}_N to denote an N -dimensional identity matrix.

II. SYSTEM MODEL AND PROBLEM FORMULATION

A. HISAC Transceiver Architecture

As shown in Fig. 1, we consider multi-user communication and multi-target sensing with the assistance of HISs. We introduce an HISAC system consisting of a transmit HIS \mathcal{P}_S and a receive HIS \mathcal{P}_R . The aperture size for both HISs is $A_T = L_x L_y$, where L_x and L_y are the lengths along x -axis and y -axis, respectively. Specifically, \mathcal{P}_S sends signals to perform multi-target sensing and communicate to K single-antenna users simultaneously, while \mathcal{P}_R receives the radar echoes from M targets. The structure of the HISAC transceiver operation is depicted in Fig. 2. The communication data streams and sensing streams are modulated into the transmit pattern at \mathcal{P}_S . Similarly, the echoed signals from M targets are received by \mathcal{P}_R , and then demodulated by M receive patterns.

Let $\mathbf{x} = [\mathbf{c}^T, \mathbf{s}^T]^T$, where $\mathbf{c} = [c_1, \dots, c_K]^T \sim \mathcal{CN}(0, \mathbf{I}_K)$ and $\mathbf{s} = [s_1, \dots, s_M]^T \sim \mathcal{CN}(0, \mathbf{I}_M)$ are communication data streams and sensing streams, respectively. Correspondingly, the transmit pattern at point p of the surface is defined as $\boldsymbol{\rho}(p) = [\rho_1, \dots, \rho_{K+M}]^H$. The pattern generated by the communication data streams is given by $j_c(p) = \sum_{k=1}^K c_k \rho_k(p)$ [19]. Similarly, the pattern generated by the sensing streams is

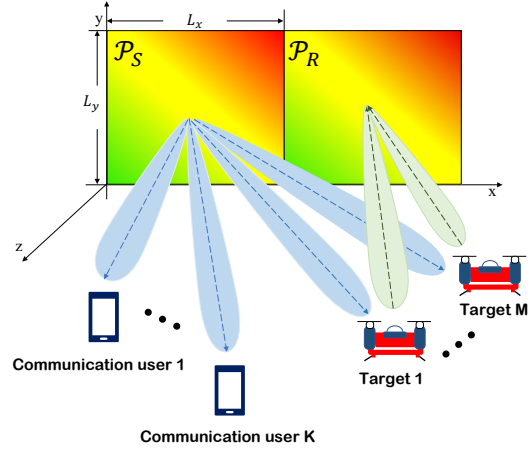


Fig. 1. The geometry of the HISAC system.

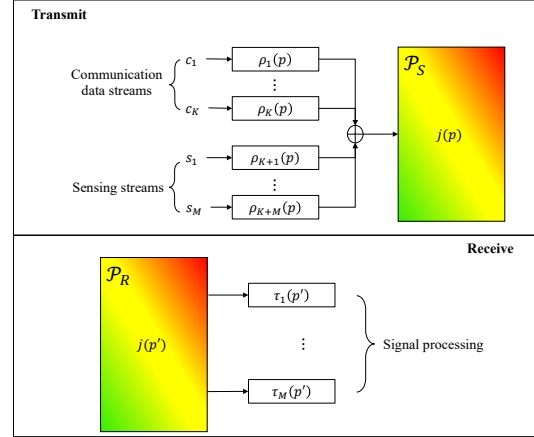


Fig. 2. Illustration of the proposed HISAC transceiver structure.

given as $j_r(p) = \sum_{m=1}^M s_m \rho_{K+m}(p)$. The combined pattern at \mathcal{P}_S is given by

$$j(p) = \sum_{k=1}^K c_k \rho_k(p) + \sum_{m=1}^M s_m \rho_{K+m}(p) = \boldsymbol{\rho}^H(p) \mathbf{x}. \quad (1)$$

Similar to the transmit end, the received signal is filtered by a set of receive patterns $\boldsymbol{\tau} = [\tau_1, \dots, \tau_M]^H$ at \mathcal{P}_R to extract the target information.

The main purpose of the HISAC system design is to achieve maximal sensing performance while ensuring multi-user communication. To support multi-target sensing and multi-user communication, both the transmit pattern $\boldsymbol{\rho}$ and receive pattern $\boldsymbol{\tau}$ need to be optimized. We consider SINR as the performance metric of both communication and sensing, described as follows.

B. Communications and Radar Performances

Let $G_k(p) \triangleq G(p'_k, p)$ be the Green's function from the source p to the user k . Based on the principle of EM propagation theory, the electric field in the space domain is

determined by ρ over surface D . The received signal at user k can be calculated by [35]

$$e_k = j\kappa Z_0 \int_D G_k(p) \rho_k(p) c_k dp + \underbrace{\sum_{i=1, i \neq k}^{K+M} j\kappa Z_0 \int_D G_k(p) \rho_i(p) x_i dp}_{\text{Interference}} + v_c, \quad k = 1, \dots, K, \quad (2)$$

where v_c is the additive white Gaussian noise (AWGN) with variance σ_c^2 , κ is the wavenumber, and Z_0 is the wave impedance in the free space. The communications SINR of the k -th user is given by

$$\eta_c(\rho; k) = \frac{\mathbf{E} \left(\left| j\kappa Z_0 \int_D G_k(p) \rho_k(p) c_k dp \right|^2 \right)}{\mathbf{E} \left(\left| \sum_{i=1, i \neq k}^{K+M} j\kappa Z_0 \int_D G_k(p) \rho_i(p) x_i dp \right|^2 \right) + \sigma_c^2}, \quad k = 1, \dots, K. \quad (3)$$

In our considered HISAC system, both communication data streams and radar streams are utilized to support multi-target sensing since they are perfectly known by the \mathcal{P}_R . Considering both transmit and receive patterns, the sensing SINR is formulated in the following.

Let $G_m(p) \triangleq G(p'_m, p)$ and $G_m^*(p) \triangleq G(p, p'_m)$ denote the Green's function from source p to m -th targets and from the m -th targets to source p , respectively. The m -th target's echo at p' is expressed as

$$y_m(p') = \alpha_m G_m^*(p) e_m, \quad m = 1, \dots, M, \quad p' \in \mathcal{P}_R, \quad (4)$$

where $e_m = j\kappa Z_0 \int_D G_m(p) \rho(p) x dp$, and α_m is the backscattering intensity of the m -th target. For ease of presentation and without loss of generality, each target's backscattering intensity is considered the same and ignored in the following.

Similarly, the received field at \mathcal{P}_R is determined by τ over surface D . Then, the received signal with respect to the l -th target is given by

$$\begin{aligned} y_l &= \sum_{m=1}^M \int_D \tau_l(p') y_m(p') dp' + \int_D \tau_l v_r(p') dp' \\ &= e_l \int_D \tau_l(p') G_l^*(p) dp' + \underbrace{\sum_{m=1, m \neq l}^M e_m \int_D \tau_l(p') G_m^*(p) dp'}_{\text{Interference}} \\ &\quad + \int_D \tau_l v_r(p') dp', \quad l = 1, \dots, M, \end{aligned} \quad (5)$$

where $v_r(p')$, $p' \in D$ is the AWGN at \mathcal{P}_R with variance σ_r^2 . Therefore, the corresponding sensing SINR is given by

$$\eta_r(\rho, \tau; l) = \frac{\mathbf{E} \left(\left| e_l \int_D \tau_l(p') G_l^*(p) dp' \right|^2 \right)}{\mathbf{E} \left(\left| \sum_{m=1, m \neq l}^M e_m \int_D \tau_l(p') G_m^*(p) dp' \right|^2 \right) + \sigma_r^2}, \quad l = 1, \dots, M. \quad (6)$$

C. Problem Formulation in Continuous Domain

From (3) and (6), both the sensing and communication SINRs rely on ρ . Meanwhile, the sensing SINR is affected by τ . Here, we aim to strike a performance trade-off between sensing and communication in the proposed HISAC system. Specifically, we propose to maximize the minimal sensing SINR among multiple targets while guaranteeing the multi-user communication SINR requirement. The resulting problem w.r.t. the continuous pattern design is formulated as

$$\max_{\rho, \tau} \min_{l=1, \dots, M} \eta_r(\rho, \tau; l), \quad (7a)$$

$$\text{s.t. } \eta_c(\rho; k) \geq \Gamma_c, \quad k = 1, \dots, K, \quad (7b)$$

$$\int_D \|\rho(p)\|_2^2 dp \leq P_T, \quad (7c)$$

$$\int_D \|\tau_l(p')\|_2^2 dp' = 1, \quad l = 1, \dots, M. \quad (7d)$$

The primary goal of (7) is to balance the sensing SINR among radar targets, and (7b) is the communication constraint for multiple users, where Γ_c represents the minimal required communication SINR. Concerning power constraints, (7c) and (7d) represent the power budget for the transmit pattern at \mathcal{P}_S and the unit-power constraint for the receive pattern at \mathcal{P}_R , respectively.

Due to the infinite dimension integrals in the objective and constraints of the problem (7), classical beamforming techniques for discrete-array-based ISAC systems are not applicable. To address these infinite dimension functions in problem (7), we develop a continuous-discrete transformation inspired by the Fourier transform, detailed in the following section.

III. CONTINUOUS-DISCRETE TRANSFORMATION

In this section, we describe the continuous-discrete transformation to solve the challenging problem in (7). The key idea is to use the Fourier transform to convert the pattern from the continuous domain into a discrete wavenumber domain. Specifically, we formulate a comprehensive continuous-discrete transformation for ρ , which is then applied to derive the expressions for communication and sensing SINRs. Based on this transformation, we approximate the continuous pattern design in (7) into a joint transmit-receive beamforming problem in the discrete domain.

A. Comprehensive Continuous-Discrete Transformation

Due to the continuity of pattern at HIS, we first transform patterns into discrete domains. For an integrable ρ defined over surface D , $\rho(p)$ can be equivalently converted from the space domain into the wavenumber domain as [35]

$$\rho_i(p) = \sum_n^{\infty} w_{i,n} \Psi_n(p), \quad i = 1, \dots, K + M, \quad (8)$$

where $w_{i,n}$ is the coefficient of the i -th pattern projected to the n -th Fourier transform function $\Psi_n(p)$. By substituting (8) into (2), the electric field is represented by

$$e(p') = j\kappa Z_0 \sum_{i=1}^{K+M} \sum_n^{\infty} x_i w_{i,n} f_{2D}^n(G_{p'}) + v_c, \quad (9)$$

where $f_{2D}^n(G_{p'}) \triangleq \int_D G(p', p) \Psi_n(p) dp$ is the Green's function Fourier transform over surface D .

To overcome the integral functions in the pattern design, we provide a closed-form expression for $f_{2D}^n(G_{p'})$ in the following proposition.

Proposition 1: Let $n = (n_x, n_y)$ denote the order along the x -axis and y -axis, and (s_x, s_y) be a source point at the surface D . Given the spatial Fourier transform function [19],

$$\Psi_n(p) = \frac{1}{\sqrt{A_T}} e^{-j2\pi\left(\frac{n_x}{L_x}(s_x - \frac{L_x}{2})\right)} e^{-j2\pi\left(\frac{n_y}{L_y}(s_y - \frac{L_y}{2})\right)}, \quad (10)$$

a closed-form expression for $f_{2D}^n(G_{p'})$ of the target (r, θ, ψ) on the far-field is

$$f_{2D}^n(G_{p'}) = \frac{e^{jk_r r} \sqrt{A_T}}{4\pi r} e^{j(n_x + n_y)\pi} \text{sinc}\left(\kappa_x^n \frac{L_x}{2}\right) \text{sinc}\left(\kappa_y^n \frac{L_y}{2}\right), \quad (11)$$

where $\kappa_x^n = \kappa \left(\sin\theta \cos\psi + \lambda \frac{n_x}{L_x}\right)$ and $\kappa_y^n = \kappa \left(\sin\theta \sin\psi + \lambda \frac{n_y}{L_y}\right)$ are wavenumbers along the x -axis and y -axis, respectively.

Proof: See Appendix A. ■

The above proposition provides an explicit expression for Green's function Fourier transform on the far-field, which we leverage to substitute the integral terms in communication and sensing SINRs.

B. Representation of Communication and sensing SINRs

Based on the previous transformation, the communication SINR can be described as follows. Combining (11) with (2), the received signal at user k is calculated as

$$\hat{e}_k = j\kappa Z_0 \sum_{i=1}^{K+M} \sum_n x_i w_{i,n} f_{2D}^n(G_k) + v_c, \quad k = 1, \dots, K. \quad (12)$$

According to [12], [35], the channel gain $\sum_n f_{2D}^n(G_k)$ within the band of $[-\kappa, \kappa]$ dominates the radiation power over the Fourier wavenumber domain. Based on Proposition 1, the wavenumber (κ_x^n, κ_y^n) is determined by the Fourier expansion order $n = (n_x, n_y)$. Thus, when the corresponding wavenumbers of the truncation order N satisfy $\kappa_x^n \geq \kappa$ and $\kappa_y^n \geq \kappa$, the Fourier series $f_{2D}^n(G_k)$ can be approximated up to the N -th order, comprising vector

$$\mathbf{f}_k = [f_{2D}^1(G_k), \dots, f_{2D}^N(G_k)]^H, \quad k = 1, \dots, K. \quad (13)$$

For convenience, we also collect the coefficients of the i -th pattern into a vector (beamformer)

$$\mathbf{w}_i = [w_{i,1}, \dots, w_{i,N}]^H, \quad i = 1, \dots, K + M. \quad (14)$$

Then, the beamforming matrix \mathbf{W} of the whole pattern is

expressed by

$$\mathbf{W} = [\mathbf{W}_c, \mathbf{W}_r], \quad (17)$$

where $\mathbf{W}_c \triangleq [\mathbf{w}_1, \dots, \mathbf{w}_K]$ and $\mathbf{W}_r \triangleq [\mathbf{w}_{K+1}, \dots, \mathbf{w}_{K+M}]$ are the beamforming matrices for communication data streams and sensing streams, respectively. By combining equations (12), (13), (14), and (17), we approximate the received signal at the k -th user as

$$\begin{aligned} \mathcal{E}_k = & j\kappa Z_0 \mathbf{f}_k^H \mathbf{w}_k c_k + \underbrace{\sum_{i=1, i \neq k}^K j\kappa Z_0 \mathbf{f}_k^H \mathbf{w}_i c_i}_{\text{Multi-user Interference}} \\ & + \underbrace{j\kappa Z_0 \mathbf{f}_k^H \mathbf{W}_r \mathbf{s}}_{\text{Sensing Interference}} + v_c, \quad k = 1, \dots, K. \end{aligned} \quad (18)$$

Therefore, the SINR at the k -th user is expressed by (15).

Similar to the transmit end, the receive pattern in the continuous space domain is converted into the discrete Fourier domain by $\tau_l(p') = \sum_n q_{l,n} \Phi_n(p)$, where $q_{l,n}$ is the coefficient of the l -th receive pattern projected to $\Phi_n(p)$. We confine the Fourier series $g_{2D}^n(G_m^*)$ over surface \mathcal{P}_R to the N -th order and comprise vector $\mathbf{g}_m^* = [g_{2D}^1(G_m^*), \dots, g_{2D}^N(G_m^*)]^H$. The coefficients of the l -th pattern are collected into a vector $\mathbf{q}_l = [q_{l,1}, \dots, q_{l,N}]^H$. Combining (11) with (5), the received echo w.r.t. the l -th target is approximated as

$$\begin{aligned} \mathcal{Y}_l = & \underbrace{j\kappa Z_0 \mathbf{q}_l^H \mathbf{G}_l \mathbf{W} \mathbf{x}}_{\text{Target echo}} + \underbrace{\sum_{m=1, m \neq l}^M j\kappa Z_0 \mathbf{q}_l^H \mathbf{G}_m \mathbf{W} \mathbf{x}}_{\text{Interference echo}} \\ & + \underbrace{\mathbf{q}_l^H \mathbf{v}_r}_{\text{Beamformer Noise}}, \quad l = 1, \dots, M, \end{aligned} \quad (19)$$

where $\mathbf{G}_m = \mathbf{g}_m \mathbf{g}_m^H$, and $\mathbf{v}_r \sim \mathcal{CN}(0, \sigma_r^2 \mathbf{I}_N)$ is the Fourier transform of v_r over surface D .

With unit-power beamformer \mathbf{q}_l at \mathcal{P}_R , the corresponding sensing SINR w.r.t. the l -th target is then expressed as (16).

C. Problem Formulation in Discrete Domain

From (15) and (16), both the sensing and communication SINRs are converted into the discrete domain and determined by transmit beamformers in \mathbf{W} and receive beamformers collected in $\mathbf{Q} = [\mathbf{q}_1, \dots, \mathbf{q}_M]$. The original problem in (7) is converted from the continuous domain into the discrete domain. Based on the transformation in Section III-A and truncation in Section III-B, the resulting approximated problem w.r.t. the joint transmit-receive beamforming can be formulated

$$\eta_c(\mathbf{W}; k) = \frac{\mathbf{f}_k^H \mathbf{w}_k \mathbf{w}_k^H \mathbf{f}_k}{\mathbf{f}_k^H \mathbf{W} \mathbf{W}^H \mathbf{f}_k - \mathbf{f}_k^H \mathbf{w}_k \mathbf{w}_k^H \mathbf{f}_k + \frac{\sigma_c^2}{\kappa^2 Z_0^2}}, \quad k = 1, \dots, K. \quad (15)$$

$$\eta_r(\mathbf{W}, \mathbf{q}_l; l) = \frac{\mathbf{q}_l^H \mathbf{G}_l \mathbf{W} \mathbf{W}^H \mathbf{G}_l^H \mathbf{q}_l}{\mathbf{q}_l^H \left(\sum_{m=1}^M \mathbf{G}_m \mathbf{W} \mathbf{W}^H \mathbf{G}_m^H - \mathbf{G}_l \mathbf{W} \mathbf{W}^H \mathbf{G}_l^H \right) \mathbf{q}_l + \frac{\sigma_r^2}{\kappa^2 Z_0^2}}, \quad l = 1, \dots, M. \quad (16)$$

as

$$\max_{\mathbf{W}, \mathbf{Q}} \min_{l=1, \dots, M} \eta_r(\mathbf{W}, \mathbf{q}_l; l), \quad (20a)$$

$$\text{s.t. } \eta_c(\mathbf{W}; k) \geq \Gamma_c, \quad k = 1, \dots, K, \quad (20b)$$

$$\|\mathbf{W}\|_F^2 \leq P_T, \quad (20c)$$

$$\|\mathbf{q}_l\|_2^2 = 1, \quad l = 1, \dots, M, \quad (20d)$$

where $\eta_r(\mathbf{W}, \mathbf{q}_l; l)$ and $\eta_c(\mathbf{W}; k)$ are defined by (16) and (15), respectively. In [19], the authors provide a methodology for computing the physical radiation power for a given surface configured by multiple patterns. The total transmit power of transmit patterns can be upper-bounded by [19]

$$\int_D \|\rho(p)\|_2^2 dp = \|\mathbf{W}\|_F^2 \leq P_T. \quad (21)$$

In (20d), the unit-power requirement for receive beamformers at \mathcal{P}_R is indicated.

Due to the non-convex max-min objective function and coupled optimized variables in objective and constraints, (20) is non-convex and challenging to solve. To circumvent the difficulties, we develop an efficient AO algorithm to address the joint transmit-receive beamforming in the HISAC system. Specifically, the ABS is proposed to accelerate the convergence of the SDR-based bisection search in the transmit beamforming, and a Rayleigh quotient-based method is developed for the receive beamformer design.

IV. JOINT TRANSMIT-RECEIVE BEAMFORMING IN HISAC SYSTEM

We begin with introducing the transmit HIS beamforming in Section IV-A, which we then utilize to design the receive beamforming with fixed transmit beamforming in Section IV-B.

A. HIS Transmit Beamforming with Fixed Receive Beamforming

In this section, we optimize the transmit beamforming matrix \mathbf{W} with fixed receive beamforming matrix \mathbf{Q} . In particular, we propose a SDR-based algorithm to obtain the optimal solution of (20) iteratively. Then, we develop an ABS method to efficiently accelerate the convergence speed.

1) *SDR-Based Algorithm*: For the convenience of analysis, we rewrite the SINR of the sensing and communication in terms of the covariance matrix \mathbf{R} , represented by

$$\begin{aligned} \eta_c(\mathbf{R}; k) &= \frac{\mathbf{f}_k^H \mathbf{R}_k \mathbf{f}_k}{\mathbf{f}_k^H (\mathbf{R} - \mathbf{R}_k) \mathbf{f}_k + \frac{\sigma_r^2}{\kappa^2 Z_0^2}}, \quad k = 1, \dots, K, \\ \eta_r(\mathbf{R}; l) &= \frac{\mathbf{q}_l^H \mathbf{G}_l \mathbf{R} \mathbf{G}_l^H \mathbf{q}_l}{\mathbf{q}_l^H \left(\sum_{m=1}^M \mathbf{G}_m \mathbf{R} \mathbf{G}_m^H - \mathbf{G}_l \mathbf{R} \mathbf{G}_l^H \right) \mathbf{q}_l + \frac{\sigma_r^2}{\kappa^2 Z_0^2}}, \quad (22) \\ & \quad l = 1, \dots, M, \end{aligned}$$

where $\mathbf{R}_k = \mathbf{w}_k \mathbf{w}_k^H$ and $\mathbf{R} = \mathbf{W} \mathbf{W}^H$. With the given receive beamformer $\mathbf{Q} = [\mathbf{q}_1, \dots, \mathbf{q}_M]$, we propose to maximize the minimal sensing SINR by optimizing the total covariance

matrix \mathbf{R} and its sub-element \mathbf{R}_k . Then, the transmit beamforming design problem is rewritten as

$$\max_{\mathbf{R}, \mathbf{R}_1, \dots, \mathbf{R}_K} \min_{l=1, \dots, M} \eta_r(\mathbf{R}; l), \quad (23a)$$

$$\text{s.t. } \eta_c(\mathbf{R}; k) \geq \Gamma_c, \quad k = 1, \dots, K, \quad (23b)$$

$$\mathbf{R} \succeq 0, \quad (23c)$$

$$\mathbf{R}_k \succeq 0, \quad k = 1, \dots, K, \quad (23d)$$

$$\mathbf{R} - \sum_{k=1}^K \mathbf{R}_k \succeq 0, \quad (23e)$$

$$\text{tr}(\mathbf{R}) \leq P_T, \quad (23f)$$

$$\text{rank}(\mathbf{R}_k) = 1, \quad k = 1, \dots, K. \quad (23g)$$

The transmit beamforming design problem outlined above is still non-convex. To deal with it, we first omit the rank-one constraints and transform (23) into a series of feasibility-checking [39] sub-problems by SDR as

$$\max_{\mathbf{R}, \mathbf{R}_1, \dots, \mathbf{R}_K, \Gamma_r} \Gamma_r, \quad (24a)$$

$$\text{s.t. } \eta_r(\mathbf{R}; l) \geq \Gamma_r, \quad l = 1, \dots, M, \quad (24b)$$

$$\eta_c(\mathbf{R}; k) \geq \Gamma_c, \quad k = 1, \dots, K, \quad (24c)$$

$$\mathbf{R} \succeq 0, \quad (24d)$$

$$\mathbf{R}_k \succeq 0, \quad k = 1, \dots, K, \quad (24e)$$

$$\mathbf{R} - \sum_{k=1}^K \mathbf{R}_k \succeq 0, \quad (24f)$$

$$\text{tr}(\mathbf{R}) \leq P_T, \quad (24g)$$

where Γ_r is an auxiliary variable to replace the minimal sensing SINR in the objective function.

Due to the fractional terms in constraints (24b) and (24c), the above problem is still non-convex. Let $\mathbf{U}_{l,m} = \mathbf{G}_m^H \mathbf{q}_l \mathbf{q}_l^H \mathbf{G}_m$, $\mathbf{F}_k = \mathbf{f}_k \mathbf{f}_k^H$. By fixing Γ_r and rearranging (24b) and (24c) as

$$(1 + \Gamma_r^{-1}) \text{tr}(\mathbf{U}_{l,l} \mathbf{R}) - \sum_{m=1}^M \text{tr}(\mathbf{U}_{l,m} \mathbf{R}) \geq \frac{\sigma_r^2}{\kappa^2 Z_0^2}, \quad (25)$$

and

$$(1 + \Gamma_c^{-1}) \text{tr}(\mathbf{F}_k \mathbf{R}_k) - \text{tr}(\mathbf{F}_k \mathbf{R}) \geq \frac{\sigma_c^2}{\kappa^2 Z_0^2}, \quad (26)$$

respectively. (24) becomes a convex semidefinite programming (SDP) feasibility-checking problem and can be solved by off-the-shelf toolbox such as CVX [40]. By providing a potential range for Γ_r that contains the optimal Γ_r^* , (24) can be solved by checking its feasibility with Γ_r being chosen in a bisection manner. Specifically, we perform a bisection search over the interval $[\Gamma_{r,start}, \Gamma_{r,end}]$, as shown in Algorithm 1.

Suppose the optimal solution $\hat{\mathbf{R}}_1, \dots, \hat{\mathbf{R}}_K$ of (24) are exactly rank-one. In that case, the relaxation used in SDR is tight, i.e., the solution to (24) coincides with the original non-convex problem (23). If the rank-one requirement is not fulfilled, the following proposition enables us to reconstruct the rank-one solution for the original problem and generate the communication beamformer $\hat{\mathbf{W}}_c = [\hat{\mathbf{w}}_1, \dots, \hat{\mathbf{w}}_K]$ and sensing beamformer $\hat{\mathbf{W}}_r$, respectively.

Proposition 2: Let $\hat{\mathbf{R}}_1, \dots, \hat{\mathbf{R}}_K, \hat{\mathbf{R}}$ be the optimal solution

Algorithm 1 Bisection Search with SDR

Input: Γ_c .

- 1: Determine $\Gamma_{r,start} = 0, \Gamma_{r,end} = \frac{\kappa^2 Z_0^2 P_T A_T}{\sigma_r^2}$.
- 2: **repeat**
- 3: Update $\Gamma_r \leftarrow \frac{1}{2} (\Gamma_{r,start} + \Gamma_{r,end})$.
- 4: Solve (24) by checking its feasibility with Γ_r . If (24) is feasible, $\Gamma_{r,start} \leftarrow \Gamma_r$; otherwise $\Gamma_{r,end} \leftarrow \Gamma_r$.
- 5: **until** $\Gamma_{r,end} - \Gamma_{r,start} \leq \epsilon_1$
- 6: Update the minimal sensing SINR as $\Gamma_{r,start}$.
- 7: Calculate $\mathbf{R}, \mathbf{R}_1, \dots, \mathbf{R}_K$ by solving (24) with $\Gamma_{r,start}$.

Output: $\mathbf{R}, \mathbf{R}_1, \dots, \mathbf{R}_K$.

of (23), each entry of the communication beamforming matrix $\hat{\mathbf{W}}_c$ is calculated by

$$\hat{\mathbf{w}}_k = \left(\mathbf{f}_k^H \hat{\mathbf{R}}_k \mathbf{f}_k \right)^{-\frac{1}{2}} \hat{\mathbf{R}}_k \mathbf{f}_k, \quad k = 1, \dots, K, \quad (27)$$

and the beamforming matrix $\hat{\mathbf{W}}_r$ for multi-target sensing is choosing by

$$\hat{\mathbf{W}}_r \hat{\mathbf{W}}_r^H = \hat{\mathbf{R}} - \sum_{k=1}^K \hat{\mathbf{R}}_k. \quad (28)$$

The optimal solution $\bar{\mathbf{R}}_1, \dots, \bar{\mathbf{R}}_K$ for (20) is reconstructed as $\bar{\mathbf{R}}_k = \hat{\mathbf{w}}_k \hat{\mathbf{w}}_k^H$, for $k = 1, \dots, K$, which is exactly rank-one and optimal.

Proof: See Appendix B. ■

It is noteworthy that, for different HISAC system setups, the dynamic searching range for potential values of feasible Γ_r changes rapidly, leading to high overhead. To overcome this challenge, we propose an ABS method which is detailed in the following, which provides a refined/shrunk searching range for Γ_r to accelerate the convergence of Algorithm 1.

2) *Adaptive Bisection Searching Method:* The main concept of ABS is to find a smaller range for feasible Γ_r , thereby accelerating convergence. For convenience, we rewrite the constraint (25) with an indicator t , given by

$$(1 + \Gamma_r^{-1}) \text{tr}(\mathbf{U}_{l,l} \mathbf{R}) - \sum_{m=1}^M \text{tr}(\mathbf{U}_{l,m} \mathbf{R}) - \sigma_R^2 \geq t, \quad (29)$$

where the equivalent noise is represented by $\sigma_R^2 = \frac{\sigma^2}{\kappa^2 Z_0^2}$. The objective function in (24) is then converted into finding the maximal t under the fixed Γ_r , which satisfies the inequality in (29). Subsequently, we employ the indicator t to evaluate the feasibility of the given Γ_r for the problem (24).

First, for the initial point of the ABS, we define the maximal potential value of the Γ_r as $\Gamma_{r,start}$, satisfying

$$\Gamma_{r,start} = \frac{P_T A_T}{\sigma_R^2} - K \Gamma_c, \quad (30)$$

where $\frac{P_T A_T}{\sigma_R^2}$ is the system's upper bound in the absence of interference-noise, and $K \Gamma_c$ is interference from the multi-user communication. Given $\Gamma_{r,start}$, (24) can be solved with SDPT3 [40], and the indicator t is computed by (29). Intuitively, when $t \geq 0$, the actual lower bound of the feasibility solution surpasses the given $\Gamma_{r,start}$, whereas when $t \leq 0$, the actual lower bound of the feasibility solution falls below the given

Algorithm 2 Adaptive Bisection Searching Method

Input: Γ_c .

Initial point: $\Gamma_{r,start} = \frac{P_T A_T}{\sigma_R^2} - K \Gamma_c$.

- 1: **while** 1 **do**
- 2: Compute the indicator t with fixed $\Gamma_{r,start}$ via (29).
- 3: If $t \geq 0$, break; otherwise $\Gamma_{r,start} \leftarrow \Gamma_{r,start} - \Gamma_c$.
- 4: **end while**
- 5: $\Gamma_{r,end} \leftarrow \Gamma_{r,start} + \Gamma_c$.
- 6: **while** 1 **do**
- 7: Compute the indicator t with fixed $\Gamma_{r,end}$ via (29).
- 8: If $t \leq 0$, break; otherwise $\Gamma_{r,end} \leftarrow \Gamma_{r,end} + \Gamma_c$.
- 9: **end while**
- 10: $\Gamma_{r,start} \leftarrow \Gamma_{r,end} - \Gamma_c$.

Output: $[\Gamma_{r,start}, \Gamma_{r,end}]$.

$\Gamma_{r,start}$. Consequently, with the guidance of t , a refined range for Γ_r can be obtained by iteratively modifying the initial $\Gamma_{r,start}$ with steps $\Gamma_{r,start} \rightarrow \Gamma_{r,start} - \Gamma_c$.

In addition, we define the end point of the potential range as $\Gamma_{r,end} = \Gamma_{r,start} + \Gamma_c$, which should be checked with indicator t . Similar to the initial point modification, when $t \geq 0$, the actual upper bound of the feasibility solution surpasses the given $\Gamma_{r,end}$, indicating that $\Gamma_{r,end} \rightarrow \Gamma_{r,end} + \Gamma_c$. After multiple iterations, we obtain the refined dynamic searching range for Γ_r , denoted as $[\Gamma_{r,start}, \Gamma_{r,end}]$. The detailed steps of ABS are summarized in Algorithm 2.

Finally, combined with a shrunk searching range obtained by the proposed ABS approach, the SDR-based bisection method in Algorithm 1 is employed to calculate the solution to the problem (24), with t serving as the solution indicator. Once the search range meets $\Gamma_{r,end} - \Gamma_{r,start} \leq \epsilon_1$ and $t \geq 0$, the iterative algorithm ends to obtain the optimal solution $\mathbf{R}, \mathbf{R}_1, \dots, \mathbf{R}_K$, which we then utilize to calculate the transmit beamformer \mathbf{W} via (27) and (28).

B. HIS Receive Beamforming with Fixed Transmit Beamforming

For a given transmit beamforming matrix \mathbf{W} , in order to maximize the minimal sensing SINR among all targets, (20) is converted to

$$\max_{\mathbf{Q}} \min_{l=1, \dots, M} \eta_r(\mathbf{q}_l; l), \quad (31a)$$

$$\text{s.t. } \|\mathbf{q}_l\|_2^2 = 1, l = 1, \dots, M. \quad (31b)$$

The receive beamforming design is still non-convex due to the fractional terms in the objective function. To tackle this problem, we propose a generalized Rayleigh quotient-based method.

First, since the optimization for each receive beamformer \mathbf{q}_l w.r.t. the l -th target is independent of sensing SINR of other targets, (31) can be decoupled into M sub-problems, i.e.,

$$\max_{\mathbf{q}_l} \frac{\mathbf{q}_l^H \mathbf{A}_l \mathbf{q}_l}{\mathbf{q}_l^H (\mathbf{A} - \mathbf{A}_l) \mathbf{q}_l + \frac{\sigma^2}{\kappa^2 Z_0^2}}, \quad (32a)$$

$$\text{s.t. } \|\mathbf{q}_l\|_2^2 = 1, \quad (32b)$$

where $\mathbf{A}_l = \mathbf{G}_l \mathbf{W} \mathbf{W}^H \mathbf{G}_l^H$ and $\mathbf{A} = \sum_{m=1}^M \mathbf{G}_m \mathbf{W} \mathbf{W}^H \mathbf{G}_m^H$. Then, we have the following lemma based on the generalized Rayleigh quotient [41], [42].

Lemma 1: The objective function in problem (32) can be equivalently written as

$$\max_{\mathbf{q}_l} \frac{\mathbf{q}_l^H \mathbf{B} \mathbf{q}_l}{\mathbf{q}_l^H \mathbf{C} \mathbf{q}_l}, \quad (33)$$

where $\mathbf{B} = \mathbf{A}_l$ and $\mathbf{C} = \mathbf{A} - \mathbf{A}_l + \mathbf{I} \frac{\sigma_r^2}{\kappa^2 Z_0^2}$. It is obvious that, for any given beamformer \mathbf{q}_l , we have the following results: $\mathbf{q}_l^H \mathbf{B} \mathbf{q}_l \geq 0$, $\mathbf{q}_l^H \mathbf{C} \mathbf{q}_l > 0$. Therefore, $\mathbf{B} \succeq 0$ and $\mathbf{C} \succ 0$ are positive semidefinite and positive definite matrices, respectively. Further, both \mathbf{B} and \mathbf{C} are apparently Hermitian matrices, thereby converting problem (32) into a generalized Rayleigh quotient maximization problem (33). Based on the Rayleigh quotient theory [41], [42], the optimal solution of (33) is given by

$$\mathbf{C}^{-1} \mathbf{B} \mathbf{v} = \lambda_{max} (\mathbf{C}^{-1} \mathbf{B}) \mathbf{v}, \quad (34)$$

where $\lambda_{max} (\mathbf{C}^{-1} \mathbf{B})$ is the maximal eigenvalue of $\mathbf{C}^{-1} \mathbf{B}$, and \mathbf{v} is the corresponding eigenvector.

Based on Lemma 1, the optimal receive beamformer \mathbf{q}_l is given by \mathbf{v} . The corresponding sensing SINR is $\lambda_{max} (\mathbf{C}^{-1} \mathbf{B})$.

We summarize the entire process of the proposed AO-based joint transmit-receive beamforming for HISAC system in Algorithm 3.

Algorithm 3 AO-Based Joint Transmit-Receive Beamforming for HISAC System

Input: Γ_c .

- 1: **repeat**
- 2: Determine $(\Gamma_{r,start}, \Gamma_{r,end})$ via Algorithm 2.
- 3: **repeat**
- 4: Update $\mathbf{R}, \mathbf{R}_1, \dots, \mathbf{R}_K$ via Algorithm 1.
- 5: **until** $\Gamma_{r,end} - \Gamma_{r,start} \leq \epsilon_1$
- 6: Update \mathbf{W} via (27) and (28).
- 7: Update \mathbf{q}_l via (34).
- 8: Update the minimal sensing SINR Γ_r^* .
- 9: Update $\Gamma_{r,start} \leftarrow \Gamma_r^*$.
- 10: **until** $|\Gamma_r^{*(i)} - \Gamma_r^{*(i-1)}| < \epsilon_2$

Output: \mathbf{W}, \mathbf{Q} .

Specifically, the transmit beamformers and receive beamformers are updated alternately until a given convergence tolerance between two iterative steps is met, i.e., $|\Gamma_r^{*(i)} - \Gamma_r^{*(i-1)}| < \epsilon_2$, where $\Gamma_r^{*(i)}$ and $\Gamma_r^{*(i-1)}$ denote the minimal sensing SINR in (i) -th and $(i-1)$ -th iterations, respectively.

V. NUMERICAL RESULTS

In this section, we provide numerical results to evaluate the performance of our proposed HISAC system and validate the effectiveness of the proposed algorithms.

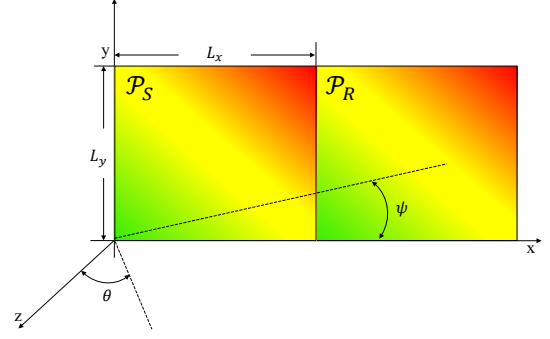


Fig. 3. Illustration of the proposed HISAC simulation scenario.

A. Simulation Setup

Without specified otherwise, the simulation parameters are summarized in Table I, and the geometry of the simulation scenario is illustrated in Fig. 3. The \mathcal{P}_S and \mathcal{P}_R are located in the XOY plane adjacently. Simultaneously, all communication users and radar targets are located on the far-field radiation region of the HIS, represented by polar coordinates. Additionally, to underscore the superiority of the proposed HISAC system, we utilize the discrete array counterpart, where antennas are deployed with half-wavelength spacing, as a baseline.

TABLE I
THE BASIC SIMULATION PARAMETERS

Parameters	Value
Center frequency	2.4 GHz
Aperture size	$A_T = 0.5 \times 0.5 \text{ m}^2$
Transmit power budget	$P_T = 100 \text{ mA}^2$
Position of the 1-th user	$(30^\circ, 180^\circ)$
Position of the 2-th user	$(30^\circ, 270^\circ)$
Position of the target 1	$(30^\circ, 90^\circ)$
Position of the target 2	$(30^\circ, 45^\circ)$
Γ_c	5 dB

Remark 1: Compared to the HIS, we assume the discrete-array-based system consists of discrete patches (isotropic source) with half-wavelength inter-distance. The aperture size of the discrete array remains the same as the HIS, allowing $D = D_x D_y = \frac{L_x}{\lambda/2} \frac{L_y}{\lambda/2}$ antennas to be optimized. According to [43], the efficient aperture size of the isotropic source is given by $\frac{\lambda^2}{4\pi}$. Therefore, the maximal radiation power of the discrete array with D elements can be calculated as $\frac{P_T A_T}{\pi}$. Based on this setup, compared to the HISAC system, the round-trip performance degradation of the discrete array counterpart is $\frac{1}{\pi^2}$.

B. Performance Evaluation

1) *Algorithm Convergence:* First, we study the convergence of the AO-based approach in Algorithm 3 and the SDR-

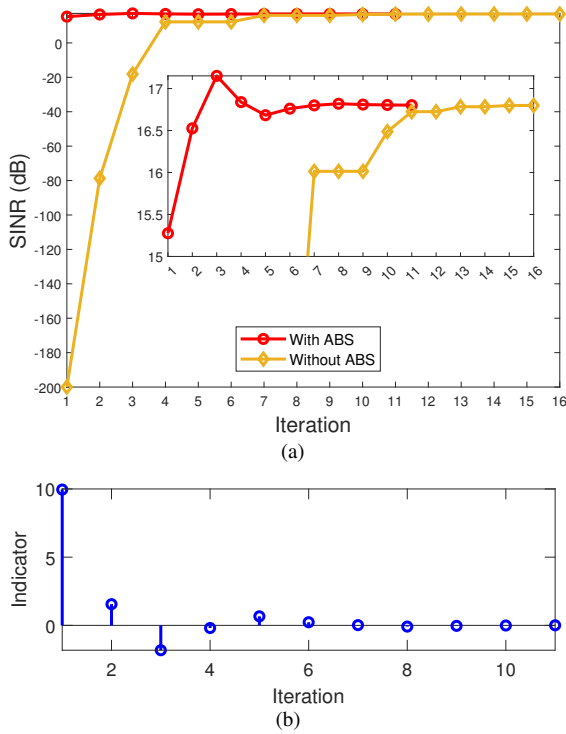


Fig. 4. Illustration of algorithm convergence. (a) Convergence of Algorithm 1 with ABS and without ABS. (b) Convergence of the indicator t .

based method in Algorithm 1 with ABS acceleration in Algorithm 2. In particular, Algorithm 3 converges within two steps, demonstrating its efficacy and robustness. Fig. 4(a) presents the convergence trends of the SDR-based method with ABS and without ABS acceleration. We can see that, with the proposed ABS in Algorithm 2, the search range of Γ_r is shrunk, accelerating the convergence of the SDR-based bisection search in Algorithm 1. Specifically, under a given convergence tolerance, the proposed algorithm converges within 11 steps, while the algorithm without ABS requires another 6 steps to reach its convergence. To evaluate the impact of the indicator t on the proposed algorithm's convergence, Fig. 4(b) shows the convergence trend of the indicator t . As can be seen, the indicator t converges to 0, implying the optimal solution to (24) is found. Specifically, when $t > 0$, the potential value Γ_r is feasible but not optimal; when $t < 0$, the potential value Γ_r is infeasible. If and only if $t \rightarrow 0$, the solution of (24) converges to the optimal value. Therefore, the minimal sensing SINR oscillates and converges to the maximal value after multiple iterations.

2) *Multi-User Single-Target Scenario*: We evaluate the performance gain of our proposed HISAC system with its discrete array counterpart and verify the effectiveness of the AO algorithm by visualizing the transmit beams. For comparison, the upper bound of sensing performance in the HISAC system is defined as the sensing SINR without communication interference, which can be calculated by $\frac{P_T A_T}{\sigma_R^2}$ via (30).

In Fig. 5, we evaluate the sensing SINR versus the maximal transmit power P_T for different ISAC configurations. We observe that our proposed HISAC system outperforms the discrete array counterpart in the considered range of power

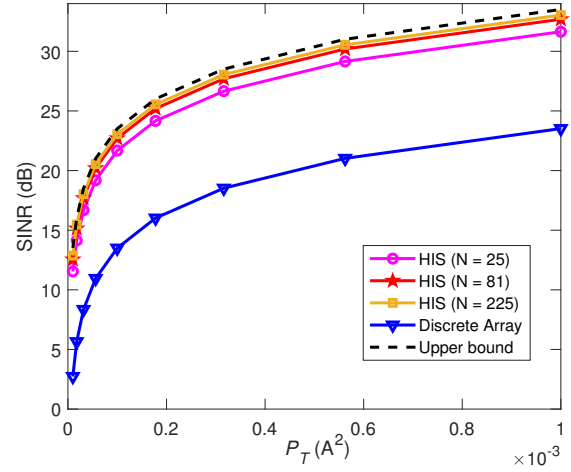


Fig. 5. Sensing SINR versus the power budget P_T .

budget. Moreover, with sufficiently large transmit power, the proposed system exhibits a 9.5 dB sensing SINR improvement compared to the discrete-array-based ISAC system. The reason is that, under the same physical aperture size, the efficient size of the discrete array is smaller than that of HIS, leading to insufficient power radiation and receiving. As stated in Remark 1, the round-trip radiation power degradation compared to HIS is π^2 , resulting in the sensing SINR undergoing 9.94 dB. Therefore, with the fulfilling capture of the HIS radiation, the performance gain of the HISAC system compared to the discrete array will stabilize around $\pi^2 \rightarrow 9.94$ dB.

To explore the impact of aperture size on the HISAC system, we evaluate the sensing SINR versus the aperture area A_T in Fig. 6, where the transmit HIS always remains a square with $L_x = L_y = \sqrt{A_T}$. As can be seen, the radar

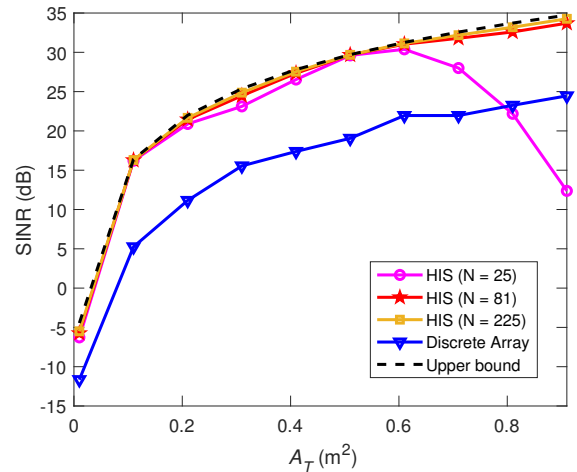


Fig. 6. Sensing SINR versus the aperture size A_T of the transmit HIS.

performance improves with the increase of the aperture size, and the sensing SINR of our proposed HISAC system exhibits a progressive enhancement as the Fourier expansion order N increases outperforming its discrete array counterpart even

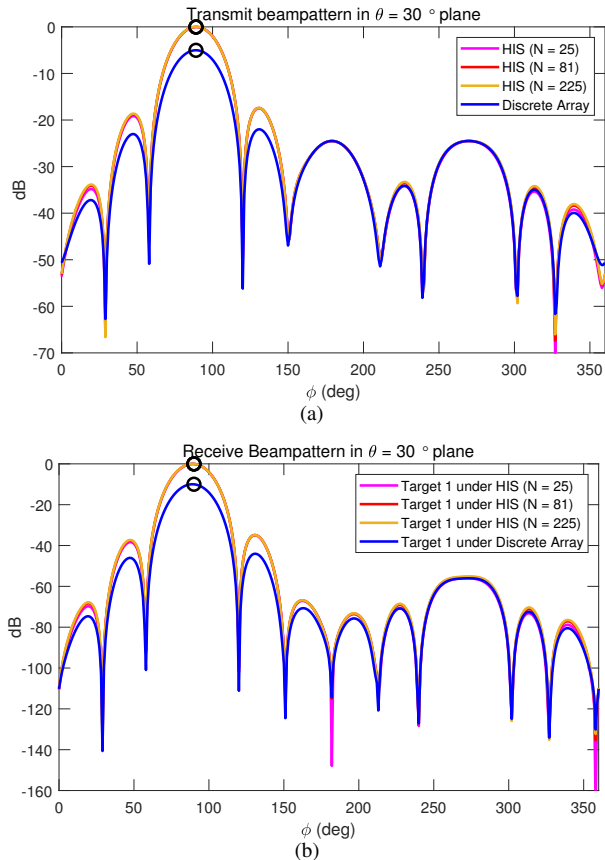


Fig. 7. HIS beampatterns for target 1. (a) Transmit beampattern. (b) Receive beampattern.

when N is moderately large. However, if the Fourier expansion order is too small and insufficient to capture the HIS radiation characteristics, the radar performance will degrade severely at the large aperture size region, potentially becoming worse than its discrete array counterpart.

In Fig. 7(a) and Fig. 7(b), we illustrate the transmit and receive beampatterns of the HIS and that of the discrete array at $\theta = 30^\circ$ plane, respectively. Based on these normalized beampatterns, we study the beampattern gain between the HIS-based and discrete-array-based system. As can be seen, in the transmit phase, as the Fourier expansion order N increases, the beamwidth of the HIS's transmit beampattern tightens, where the peak power reaches its maximum until the N is sufficient for characterizing the HIS radiation. Meanwhile, the peak value of the transmit beampattern based on the discrete array demonstrates 4.9 dB degradation compared to HIS, which agrees with π . In addition, for the receive beampattern w.r.t. target 1, the peak value of the HIS's beampattern outperforms that of the discrete array with a 9.7 dB enhancement. As a result, the sensing SINR for target 1 can be significantly improved after the receive beamforming under the proposed HISAC transceiver architecture. The reason is that both the HIS's transmit and receive beamformer are optimized at the receiver side, leading to the overall sensing SINR improvement in our proposed architecture.

In Fig. 8, we explore the sensing SINR under varying communication SINR requirement. Specifically, we evaluate

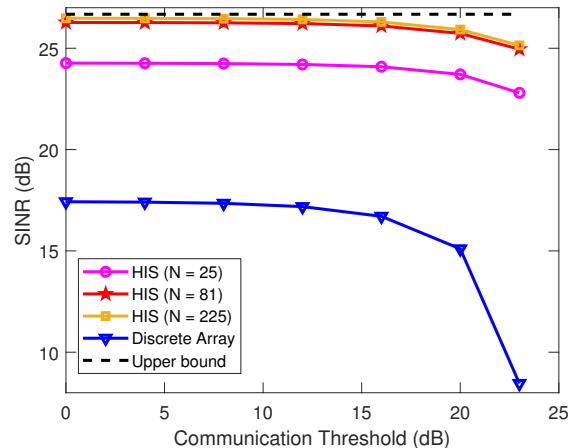


Fig. 8. Sensing SINR versus communication SINR threshold Γ_c .

sensing SINR versus different communication threshold Γ_c . The physical aperture size is $A_T = 0.6 \times 0.6 \text{ m}^2$ to demonstrate the superior sensing SINR difference between Fourier expansion order N and its discrete array counterpart. A clear trade-off between sensing and communication is presented, in which the sensing SINR decreases as the communication SINR requirement increases. In addition, we observe that our proposed HISAC system shows robustness compared to the discrete array system, possessing more significant sensing performance gain with higher communication SINR threshold. Specifically, as Γ_c increases, the sensing SINR gain of the HISAC system over the discrete array-based ISAC system increases from 7.4 dB to 15.6 dB, demonstrating the advantages of incorporating HIS into ISAC systems.

3) *Multi-User Multi-Target Scenario*: An additional radar target positioned at $(30^\circ, 45^\circ)$ is introduced in the multi-user multi-target scenario. In Fig. 9, we compare the minimal sensing SINR among radar targets for different Fourier expansion order N versus P_T . As observed, due to inter-target interference, the sensing SINR undergoes a 3 dB degradation, compared to the interference-free upper bound. Nevertheless, our proposed HISAC system still outperforms its discrete array counterpart with 9.7 dB sensing SINR enhancement. The insight here is that the number of radar targets will not affect the sensing SINR enhancement between the HIS and the discrete array. This is because the radiation power of both architectures is independent of the number/directions of targets. Therefore, when the Fourier expansion order N is sufficient, our system can still achieve power gain around π^2 .

In Fig. 10, we illustrate the normalized transmit and receive beampatterns at $\theta = 30^\circ$ plane to demonstrate the impact of multi-target sensing on the minimal sensing SINR. As observed in Fig. 10(a), the main lobe of the HIS transmit beampattern is split into two main lobes with the same peak level. Compared to the discrete array, the transmit beampattern of HIS exhibits a 4.9 dB enhancement in each direction of targets. As can be seen in Fig. 10(b), the receiving beamforming strengthens the beampattern's peak values in the

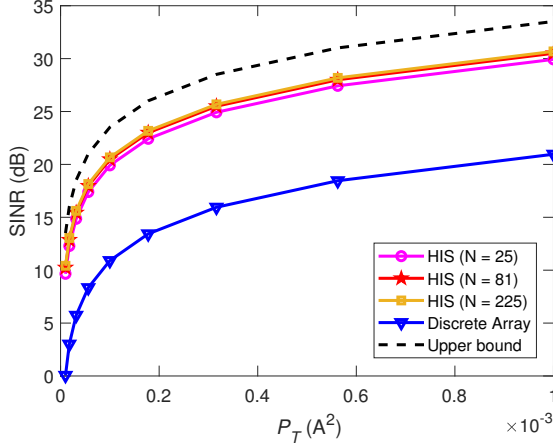


Fig. 9. Minimal sensing SINR versus the power budget P_T .

directions of targets while suppressing those of the clutters (targets located in other directions) deeply. Specifically, for the receive beamforming w.r.t. target 1, the direction w.r.t. target 1 is enhanced while the direction w.r.t. target 2 is suppressed and vice versa. Note that the peak value of HIS still maintains an enhancement around 9.7 dB compared to the discrete array, regardless of the directions of the receive beamforming. Therefore, our proposed algorithm is efficient in addressing the multi-user multi-target scenario and indicates that the sensing SINR improvement is attributed to the efficient aperture and is independent of the directions of targets.

VI. CONCLUSIONS

This paper introduced a novel concept to ISAC systems by proposing the HISAC system. Through the continuous-aperture array fabrication of both transmitter and receiver, the HISAC system presented unique challenges in design. To address these challenges, a continuous-discrete transformation technique based on the Fourier transform was employed, facilitating the conversion of continuous pattern design into discrete beamforming design. Subsequently, a joint transmit-receive beamforming optimization problem was formulated to balance multi-target sensing performance with multi-user communication requirements. An AO-based algorithm was developed to efficiently tackle the non-convex optimization problem with coupled variables. Numerical results demonstrated superior performance compared to traditional discrete-array-based ISAC systems, achieving significantly enhanced sensing capabilities while maintaining predetermined communication performance levels.

APPENDIX

A. Proof of Proposition 1

The expression of the scalar Green's function on the far-field is given by

$$G(\mathbf{r}, \mathbf{s}) = \frac{e^{j\kappa\|\mathbf{r}-\mathbf{s}\|}}{4\pi\|\mathbf{r}-\mathbf{s}\|}, \quad (\text{A.1})$$

where \mathbf{r} and \mathbf{s} are positions of the point target and source, respectively. Let $\mathbf{r} = (r, \theta, \psi)$ denote the position of p' in the

Spherical coordinate, and $\mathbf{s} = (s_x, s_y)$ be a source point at the surface in the Cartesian coordinate. The Euclidean distance in the Cartesian coordinate system is calculated as

$$\begin{aligned} \|\mathbf{r} - \mathbf{s}\| &= \sqrt{(r \sin \theta \cos \psi - s_x)^2 + (r \sin \theta \sin \psi - s_y)^2 + r^2 \cos^2 \theta} \\ &\approx r - \sin \theta (s_x \cos \psi + s_y \sin \psi). \end{aligned} \quad (\text{A.2})$$

By substituting (A.2) into (A.1), the Green's function on the far field is approximated as

$$G_{p'} = \frac{e^{j\kappa r}}{4\pi r} e^{-j\kappa s_x \sin \theta \cos \psi} e^{-j\kappa s_y \sin \theta \sin \psi}. \quad (\text{A.3})$$

Combining (A.3) and (9), the Green's function Fourier transform $f_{2D}^n(G_{p'})$, is given by

$$f_{2D}^n(G_{p'}) = \int_D \frac{e^{j\kappa r}}{4\pi r} e^{-j\kappa s_x \sin \theta \cos \psi} e^{-j\kappa s_y \sin \theta \sin \psi} \Psi_n(p) dp, \quad (\text{A.4})$$

where we decompose the n -th order $n = (n_x, n_y)$ along the x -axis and y -axis, the Fourier transform function $\Psi_n(p)$ is rewritten as

$$\Psi_n(p) = \frac{1}{\sqrt{A_T}} e^{-j2\pi\left(\frac{n_x}{L_x}\left(s_x - \frac{L_x}{2}\right)\right)} e^{-j2\pi\left(\frac{n_y}{L_y}\left(s_y - \frac{L_y}{2}\right)\right)}. \quad (\text{A.5})$$

Let $\kappa_x^n = \kappa \left(\sin \theta \cos \psi + \lambda \frac{n_x}{L_x} \right)$ and $\kappa_y^n = \kappa \left(\sin \theta \sin \psi + \lambda \frac{n_y}{L_y} \right)$ denote the wavenumbers along the x -axis and y -axis, respectively. Combining (A.4) with (A.5), the Green's function Fourier transform for arbitrary position (r, θ, ψ) is calculated as follows:

$$\begin{aligned} f_{2D}^n(G_{p'}) &= \frac{e^{j\kappa r}}{4\pi r \sqrt{A_T}} e^{j(n_x + n_y)\pi} \\ &\int_{L_x} e^{-j\kappa_x s_x} ds_x \int_{L_y} e^{-j\kappa_y s_y} ds_y \\ &= \frac{e^{j\kappa r}}{4\pi r \sqrt{A_T}} e^{j(n_x + n_y)\pi} \\ &\left[\frac{e^{-j\kappa_x^n s_x}}{-j\kappa_x^n} \right]_{-\frac{L_x}{2}}^{\frac{L_x}{2}} \left[\frac{e^{-j\kappa_y^n s_y}}{-j\kappa_y^n} \right]_{-\frac{L_y}{2}}^{\frac{L_y}{2}} \\ &= \frac{e^{j\kappa r}}{4\pi r \sqrt{A_T}} e^{j(n_x + n_y)\pi} \\ &\frac{L_x \sin\left(\kappa_x^n \frac{L_x}{2}\right)}{\kappa_x^n \frac{L_x}{2}} \frac{L_y \sin\left(\kappa_y^n \frac{L_y}{2}\right)}{\kappa_y^n \frac{L_y}{2}} \\ &= \frac{e^{j\kappa r} \sqrt{A_T}}{4\pi r} e^{j(n_x + n_y)\pi} \text{sinc}\left(\kappa_x^n \frac{L_x}{2}\right) \text{sinc}\left(\kappa_y^n \frac{L_y}{2}\right). \end{aligned} \quad (\text{A.6})$$

Finally, we get an expression of the Green's function Fourier transform for arbitrary position (r, θ, ψ) :

$$\begin{aligned} f_{2D}^n(G_{p'}) &= \frac{e^{j\kappa r} \sqrt{A_T}}{4\pi r} e^{j(n_x + n_y)\pi} \\ &\text{sinc}\left(\kappa_x^n \frac{L_x}{2}\right) \text{sinc}\left(\kappa_y^n \frac{L_y}{2}\right). \end{aligned} \quad (\text{A.7})$$

This concludes the proof.

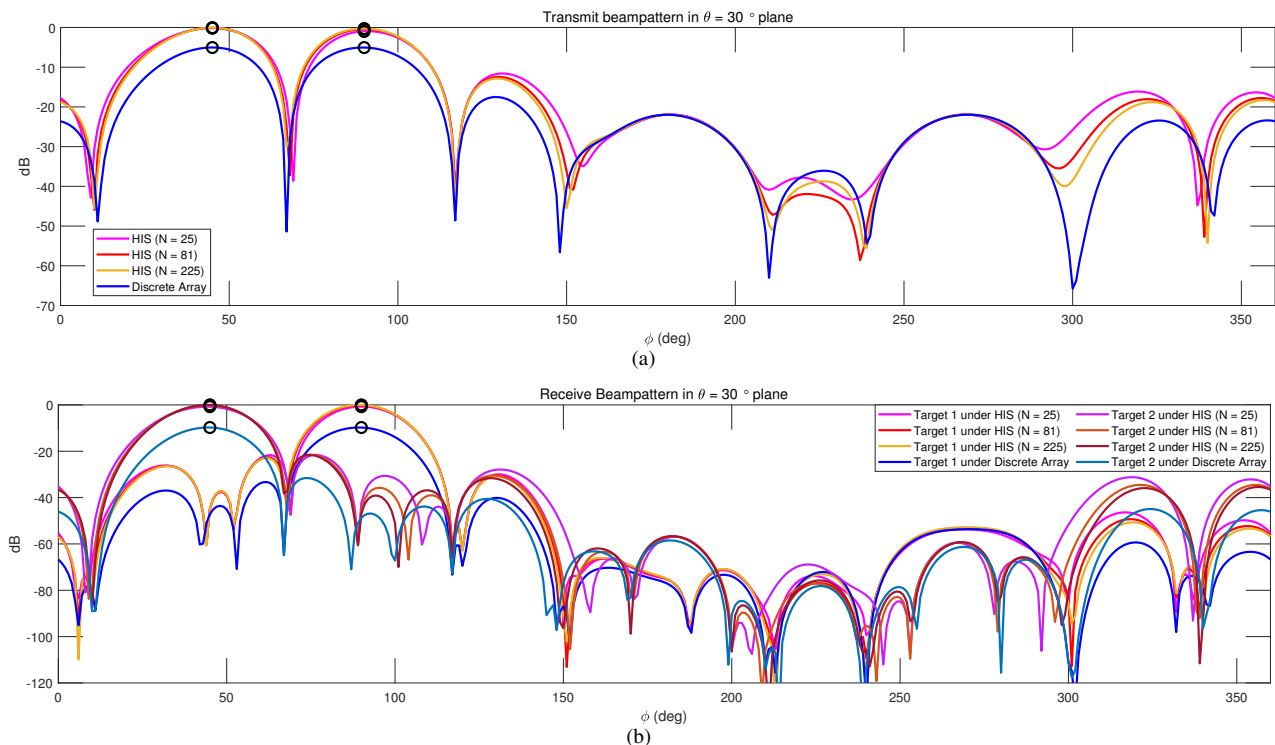


Fig. 10. HIS beampatterns for multi-target. (a) Transmit beampattern. (b) Receive beampattern.

B. Proof of Proposition 2

Let $\hat{\mathbf{R}}_1, \dots, \hat{\mathbf{R}}_K, \hat{\mathbf{R}}$ be the optimal solution of (23), each entry of the communication beamforming matrix $\hat{\mathbf{W}}_c$ is calculated by

$$\hat{\mathbf{w}}_k = \left(\mathbf{f}_k^H \hat{\mathbf{R}}_k \mathbf{f}_k \right)^{-\frac{1}{2}} \hat{\mathbf{R}}_k \mathbf{f}_k, \quad k = 1, \dots, K, \quad (\text{B.1})$$

and the beamforming matrix $\hat{\mathbf{W}}_r$ for sensing is choosing by

$$\hat{\mathbf{W}}_r \hat{\mathbf{W}}_r^H = \hat{\mathbf{R}} - \sum_{k=1}^K \hat{\mathbf{R}}_k. \quad (\text{B.2})$$

To show the beamforming solution $\hat{\mathbf{W}}_c$ and $\hat{\mathbf{W}}_r$ obtained by using (B.1) and (B.2) are solutions of (23), we need to prove that the reconstructed matrices $\bar{\mathbf{R}} = \hat{\mathbf{W}}_c \hat{\mathbf{W}}_c^H + \hat{\mathbf{W}}_r \hat{\mathbf{W}}_r^H$, $\bar{\mathbf{R}}_k = \hat{\mathbf{w}}_k \hat{\mathbf{w}}_k^H$, for $k = 1, \dots, K$, remain the same optimal and satisfy all the constraints of problem (23).

First, since the objective function in (23) is only determined by the optimal solution $\hat{\mathbf{R}}$, the objective function in (23) satisfies. Obviously, the reconstructed matrices $\bar{\mathbf{R}}_1, \dots, \bar{\mathbf{R}}_K$ are rank-one, satisfying (23g).

Then, we only need to prove that matrices $\bar{\mathbf{R}}_1, \dots, \bar{\mathbf{R}}_K$, satisfy constraints (23b), (23c). According to (B.1), we have the following equivalent formula,

$$\begin{aligned} \mathbf{f}_k^H \hat{\mathbf{w}}_k \hat{\mathbf{w}}_k^H \mathbf{f}_k &= \mathbf{f}_k^H \left(\mathbf{f}_k^H \hat{\mathbf{R}}_k \mathbf{f}_k \right)^{-1} \hat{\mathbf{R}}_k \mathbf{f}_k \mathbf{f}_k^H \hat{\mathbf{R}}_k \mathbf{f}_k \\ &\equiv \mathbf{f}_k^H \hat{\mathbf{R}}_k \mathbf{f}_k, \quad k = 1, \dots, K, \end{aligned} \quad (\text{B.3})$$

which indicates the SINR constraints (23b) for user communication are satisfied. Since the reconstructed solutions $\bar{\mathbf{R}}_k$, for $k = 1, \dots, K$, satisfy $\mathbf{f}_k^H \bar{\mathbf{R}}_k \mathbf{f}_k \equiv \mathbf{f}_k^H \hat{\mathbf{R}}_k \mathbf{f}_k \geq 0$, we have $\bar{\mathbf{R}}_k \succeq 0, \forall k$, satisfying (23c).

This concludes the proof.

REFERENCES

- [1] J. A. Zhang, F. Liu, C. Masouros, R. W. Heath, Z. Feng, L. Zheng, and A. Petropulu, "An overview of signal processing techniques for joint communication and radar sensing," *IEEE Journal of Selected Topics in Signal Processing*, vol. 15, no. 6, pp. 1295–1315, 2021.
- [2] F. Liu, Y. Cui, C. Masouros, J. Xu, T. X. Han, Y. C. Eldar, and S. Buzzi, "Integrated sensing and communications: Toward dual-functional wireless networks for 6G and beyond," *IEEE Journal on Selected Areas in Communications*, vol. 40, no. 6, pp. 1728–1767, 2022.
- [3] X. Liu, T. Huang, N. Shlezinger, Y. Liu, J. Zhou, and Y. C. Eldar, "Joint transmit beamforming for multiuser MIMO communications and MIMO radar," *IEEE Transactions on Signal Processing*, vol. 68, pp. 3929–3944, 2020.
- [4] H. Hua, J. Xu, and T. X. Han, "Optimal transmit beamforming for integrated sensing and communication," *IEEE Transactions on Vehicular Technology*, vol. 72, no. 8, pp. 10 588–10 603, 2023.
- [5] Z. He, W. Xu, H. Shen, Y. Huang, and H. Xiao, "Energy efficient beamforming optimization for integrated sensing and communication," *IEEE Wireless Communications Letters*, vol. 11, no. 7, pp. 1374–1378, 2022.
- [6] J. Wang, S. Gong, Q. Wu, and S. Ma, "RIS-aided MIMO systems with hardware impairments: Robust beamforming design and analysis," *IEEE Transactions on Wireless Communications*, vol. 22, no. 10, pp. 6914–6929, 2023.
- [7] L. Chen, Z. Wang, Y. Du, Y. Chen, and F. R. Yu, "Generalized transceiver beamforming for DFRC with MIMO radar and MU-MIMO communication," *IEEE Journal on Selected Areas in Communications*, vol. 40, no. 6, pp. 1795–1808, 2022.
- [8] F. Liu, Y.-F. Liu, A. Li, C. Masouros, and Y. C. Eldar, "Cramér-rao bound optimization for joint radar-communication beamforming," *IEEE Transactions on Signal Processing*, vol. 70, pp. 240–253, 2021.
- [9] T. Huang, N. Shlezinger, X. Xu, Y. Liu, and Y. C. Eldar, "MAJoRCOM: A dual-function radar communication system using index modulation," *IEEE Transactions on Signal Processing*, vol. 68, pp. 3423–3438, 2020.
- [10] T. Huang, N. Shlezinger, X. Xu, D. Ma, Y. Liu, and Y. C. Eldar, "Multi-carrier agile phased array radar," *IEEE Transactions on Signal Processing*, vol. 68, pp. 5706–5721, 2020.

- [11] D. Ma, N. Shlezinger, T. Huang, Y. Shavit, M. Namer, Y. Liu, and Y. C. Eldar, "Spatial modulation for joint radar-communications systems: Design, analysis, and hardware prototype," *IEEE Transactions on Vehicular Technology*, vol. 70, no. 3, pp. 2283–2298, 2021.
- [12] O. T. Demir, E. Björnson, and L. Sanguinetti, "Channel modeling and channel estimation for holographic massive MIMO with planar arrays," *IEEE Wireless Communications Letters*, vol. 11, no. 5, pp. 997–1001, 2022.
- [13] R. Deng, Y. Zhang, H. Zhang, B. Di, H. Zhang, H. V. Poor, and L. Song, "Reconfigurable holographic surfaces for ultra-massive MIMO in 6G: Practical design, optimization and implementation," *IEEE Journal on Selected Areas in Communications*, vol. 41, no. 8, pp. 2367–2379, 2023.
- [14] F. Liu and C. Masouros, "Hybrid beamforming with sub-arrayed MIMO radar: Enabling joint sensing and communication at mmwave band," in *ICASSP 2019-2019 IEEE International Conference on Acoustics, Speech and Signal Processing (ICASSP)*. IEEE, 2019, pp. 7770–7774.
- [15] G. Gradoni and M. Di Renzo, "End-to-end mutual coupling aware communication model for reconfigurable intelligent surfaces: An electromagnetic-compliant approach based on mutual impedances," *IEEE Wireless Communications Letters*, vol. 10, no. 5, pp. 938–942, 2021.
- [16] A. Pizzo, L. Sanguinetti, and T. L. Marzetta, "Fourier plane-wave series expansion for holographic MIMO communications," *IEEE Transactions on Wireless Communications*, vol. 21, no. 9, pp. 6890–6905, 2022.
- [17] A. Pizzo, T. L. Marzetta, and L. Sanguinetti, "Spatially-stationary model for holographic MIMO small-scale fading," *IEEE Journal on Selected Areas in Communications*, vol. 38, no. 9, pp. 1964–1979, 2020.
- [18] M. A. Jensen and J. W. Wallace, "Capacity of the continuous-space electromagnetic channel," *IEEE Transactions on Antennas and Propagation*, vol. 56, no. 2, pp. 524–531, 2008.
- [19] Z. Zhang and L. Dai, "Pattern-division multiplexing for multi-user continuous-aperture MIMO," *IEEE Journal on Selected Areas in Communications*, vol. 41, no. 8, pp. 2350–2366, 2023.
- [20] H. Zhang, H. Zhang, B. Di, M. D. Renzo, Z. Han, H. V. Poor, and L. Song, "Holographic integrated sensing and communication," *IEEE Journal on Selected Areas in Communications*, vol. 40, no. 7, pp. 2114–2130, 2022.
- [21] L. Wei, C. Huang, G. C. Alexandropoulos, E. Wei, Z. Zhang, M. Debbah, and C. Yuen, "Multi-user holographic MIMO surfaces: Channel modeling and spectral efficiency analysis," *IEEE Journal of Selected Topics in Signal Processing*, vol. 16, no. 5, pp. 1112–1124, 2022.
- [22] S. Hu, F. Rusek, and O. Edfors, "Beyond massive MIMO: The potential of data transmission with large intelligent surfaces," *IEEE Transactions on Signal Processing*, vol. 66, no. 10, pp. 2746–2758, 2018.
- [23] C. Huang, S. Hu, G. C. Alexandropoulos, A. Zappone, C. Yuen, R. Zhang, M. Di Renzo, and M. Debbah, "Holographic MIMO surfaces for 6G wireless networks: Opportunities, challenges, and trends," *IEEE wireless communications*, vol. 27, no. 5, pp. 118–125, 2020.
- [24] N. C. Luong, X. Lu, D. T. Hoang, D. Niyato, and D. I. Kim, "Radio resource management in joint radar and communication: A comprehensive survey," *IEEE Communications Surveys & Tutorials*, 2021.
- [25] Z. He, W. Xu, H. Shen, D. W. K. Ng, Y. C. Eldar, and X. You, "Full-duplex communication for ISAC: Joint beamforming and power optimization," *IEEE Journal on Selected Areas in Communications*, vol. 41, no. 9, pp. 2920–2936, 2023.
- [26] J. Pritzker, J. Ward, and Y. C. Eldar, "Transmit precoder design approaches for dual-function radar-communication systems," *arXiv preprint arXiv:2203.09571*, 2022.
- [27] C. Wen, Y. Huang, and T. N. Davidson, "Efficient transceiver design for MIMO dual-function radar-communication systems," *IEEE Transactions on Signal Processing*, vol. 71, pp. 1786–1801, 2023.
- [28] C. G. Tsinos, A. Arora, S. Chatzinotas, and B. Ottersten, "Joint transmit waveform and receive filter design for dual-function radar-communication systems," *IEEE Journal of Selected Topics in Signal Processing*, vol. 15, no. 6, pp. 1378–1392, 2021.
- [29] Z. Liu, H. Zhang, T. Huang, F. Xu, and Y. C. Eldar, "Hybrid RIS-assisted MIMO dual-function radar-communication system," *IEEE Transactions on Signal Processing*, vol. 72, pp. 1650–1665, 2024.
- [30] Y. Zhang, W. Ni, J. Wang, W. Tang, M. Jia, Y. C. Eldar, and D. Niyato, "Robust transceiver design for covert integrated sensing and communications with imperfect CSI," *IEEE Transactions on Communications*, pp. 1–1, 2024.
- [31] R. Deng, B. Di, H. Zhang, D. Niyato, Z. Han, H. V. Poor, and L. Song, "Reconfigurable holographic surfaces for future wireless communications," *IEEE Wireless Communications*, vol. 28, no. 6, pp. 126–131, 2021.
- [32] T. Gong, P. Gavrilidis, R. Ji, C. Huang, G. C. Alexandropoulos, L. Wei, Z. Zhang, M. Debbah, H. V. Poor, and C. Yuen, "Holographic MIMO communications: Theoretical foundations, enabling technologies, and future directions," *IEEE Communications Surveys & Tutorials*, vol. 26, no. 1, pp. 196–257, 2024.
- [33] J. An, C. Yuen, C. Huang, M. Debbah, H. Vincent Poor, and L. Hanzo, "A tutorial on holographic MIMO communications—part I: Channel modeling and channel estimation," *IEEE Communications Letters*, vol. 27, no. 7, pp. 1664–1668, 2023.
- [34] Z. Wan, J. Zhu, Z. Zhang, L. Dai, and C.-B. Chae, "Mutual information for electromagnetic information theory based on random fields," *IEEE Transactions on Communications*, vol. 71, no. 4, pp. 1982–1996, 2023.
- [35] L. Sanguinetti, A. A. D'Amico, and M. Debbah, "Wavenumber-division multiplexing in line-of-sight holographic MIMO communications," *IEEE Transactions on Wireless Communications*, vol. 22, no. 4, pp. 2186–2201, 2023.
- [36] J. Zhu, Z. Wan, L. Dai, M. Debbah, and H. V. Poor, "Electromagnetic information theory: Fundamentals, modeling, applications, and open problems," *IEEE Wireless Communications*, pp. 1–7, 2024.
- [37] H. Zhang, H. Zhang, B. Di, and L. Song, "Holographic integrated sensing and communications: Principles, technology, and implementation," *IEEE Communications Magazine*, vol. 61, no. 5, pp. 83–89, 2023.
- [38] Z. Wang, J. Zhang, H. Du, E. Wei, B. Ai, D. Niyato, and M. Debbah, "Extremely large-scale MIMO: Fundamentals, challenges, solutions, and future directions," *IEEE Wireless Communications*, pp. 1–9, 2023.
- [39] L. Zhang, R. Zhang, Y.-C. Liang, Y. Xin, and S. Cui, "On the relationship between the multi-antenna secrecy communications and cognitive radio communications," *IEEE Transactions on Communications*, vol. 58, no. 6, pp. 1877–1886, 2010.
- [40] K.-C. Toh, M. J. Todd, and R. H. Tütüncü, "SDPT3—a MATLAB software package for semidefinite programming, version 1.3," *Optimization methods and software*, vol. 11, no. 1-4, pp. 545–581, 1999.
- [41] X. Wang, Z. Fei, and Q. Wu, "Integrated sensing and communication for RIS-assisted backscatter systems," *IEEE Internet of Things Journal*, vol. 10, no. 15, pp. 13 716–13 726, 2023.
- [42] M. Zhang, Y. He, Y. Cai, G. Yu, and N. Al-Dhahir, "Design and performance analysis of wireless legitimate surveillance systems with radar function," *IEEE Transactions on Communications*, vol. 71, no. 4, pp. 2517–2531, 2023.
- [43] C. A. Balanis, *Antenna theory: analysis and design*. John Wiley & sons, 2016.